land

MDPI

Article

Two Decades of Global Cropland Fire Activity: Spatiotemporal Patterns and Regional Trends

Chenqin Lian [1,2], Zhiming Feng [2], Gangzhu Li [3,4,*] and Zhiqiang Liu [4,5]

[1] School of Public Affairs, Nanjing University of Science and Technology, Nanjing 210094, China
[2] Institute of Geographic Sciences and Natural Resources Research, Chinese Academy of Sciences, Beijing 100101, China; fengzm@igsnrr.ac.cn
[3] Inner Mongolia Key Laboratory of Mining Engineering, School of Mining and Coal, Inner Mongolia University of Science and Technology, Baotou 014010, China
[4] Autonomous Region Collaborative Innovation Center for Integrated Management of Water Resources and Water Environment in the Inner Mongolia Reaches of the Yellow River, College of Water Conservancy and Civil Engineering, Inner Mongolia Agricultural University, Hohhot 010018, China
[5] State Key Laboratory of Water Engineering Ecology and Environment in Arid Area, Hohhot 010018, China
* Correspondence: gli@imust.edu.cn

Abstract

Cropland fires constitute an important part of global biomass burning. The spatiotemporal patterns of cropland fires across the globe, especially the co-variation characteristics of fire frequency and fire radiative power (FRP), have not been fully clarified. This study quantifies global cropland fire activity from 2003 to 2022 using Moderate Resolution Imaging Spectroradiometer Collection 6.1 (MODIS C6.1) active fire products combined with land-cover datasets, adopting fire frequency and FRP (MW) as dual indicators. Spatiotemporal patterns and trends were examined across global, continental, national, and 0.25° × 0.25° grid scales using Theil–Sen slope estimation and the Mann–Kendall test. We hypothesized that global cropland fire activity exhibits pronounced spatial heterogeneity and divergent regional trajectories. The results revealed that cropland fires were geographically concentrated, with Asia and Africa accounting for nearly 70% of the global total. A global aggregated bimodal seasonality was observed, with peaks in March–April and August–October, alongside substantial regional heterogeneity. Globally, fire frequency and FRP declined significantly at −28,453 yr^{-1} and −1,268,171 MW yr^{-1} ($p < 0.001$), representing overall reductions of 41% and 49%, with prominent declines in South America, Asia, and Africa. Meanwhile, a small number of countries, such as India and the Democratic Republic of the Congo (DRC), displayed significant increasing trends. These findings provide a systematic characterization of the spatiotemporal heterogeneity of global cropland fires, offering a scientific basis for targeted fire monitoring and sustainable cropland management.

Keywords: MODIS; fire radiative power (FRP); global patterns; crop residue burning; remote sensing

Check for updates

Academic Editor: Dursun Zafer Seker

Received: 13 August 2026
Revised: 16 October 2026
Accepted: 19 October 2026
Published: 18 November 2026

Copyright: © 2026 by the authors. Licensee MDPI, Basel, Switzerland. This article is an open access article distributed under the terms and conditions of the Creative Commons Attribution (CC BY) license.

1. Introduction

Fire is an integral component of the Earth system and, since the advent of slash-and-burn cultivation, has been deliberately employed as a land management tool that persists in contemporary agricultural ecosystems [1–5]. Cropland fires are predominantly anthropogenic, with prescribed burning remaining a common method for disposing of crop residues [6–8]. Cropland fires are a major source of particulate matter and aerosols, contributing to severe haze episodes and degrading regional air quality [9]. This degradation

 https://doi.org/10.3390/land15112218

is directly linked to increased respiratory and cardiovascular morbidity, mortality, and hospitalization rates [10–12]. Although ignition is spatially confined to agricultural areas, the proximity of croplands to human settlements and the recurrence of burning cycles create transboundary environmental risks [13]. Through long-range atmospheric transport, pollutants from cropland fires can affect populations far from the source regions, extending public health threats well beyond local contexts [14]. Their environmental consequences extend beyond atmospheric emissions, air pollution, and public health [9–15] to the soils themselves. Slash-and-burn agriculture and crop-residue burning can modify soil physical, chemical, and biogeochemical properties. Such burning typically reduces porosity, aggregation, and cation exchange capacity while heightening erosion risk, with direct implications for soil fertility, organic matter, structure, and erosion processes [16,17]. Yet these soil-related dimensions have received considerably less attention in global fire assessments than atmospheric impacts, despite being particularly relevant in agricultural systems where repeated burning cycles can progressively alter the soil resource base on which long-term productivity depends [16,17]. Elucidating the spatiotemporal patterns and long-term trends of global cropland fires is therefore an important condition for understanding the full environmental footprint of this practice and for guiding its sustainable management.

Satellite remote sensing provides an essential platform for fire monitoring. The MODIS active fire product, which features a continuous two-decade observational record and validated detection performance, has become a cornerstone of cropland-fire research. [18–27]. First, although numerous studies have examined fire dynamics across all vegetation types [28], analyses dedicated specifically to global cropland fires remain limited. Second, most existing work has relied primarily on fire counts and burned area [13,29], largely omitting fire radiative power (FRP)—a direct measure of combustion intensity—so that the joint behavior of fire frequency and combustion intensity, both essential for emission estimation and fire management, remains poorly understood [30]. Third, previous analyses have been largely confined to regional or national scales [23,24,26,31], providing few comprehensive assessments of geospatial and temporal evolution at the global level. Consequently, the interplay between where cropland fires occur, when they peak, and how their frequency and intensity change over time has not been jointly characterized at the global scale, underscoring the need for an integrated multi-scale analysis that jointly leverages fire frequency and FRP.

We hypothesized that global cropland fire activity exhibits pronounced spatial heterogeneity and divergent regional trajectories. Using MODIS C6.1 active fire products and annual global land-cover data from 2003 to 2022, we quantified cropland fire dynamics at global, continental, national, and 0.25° × 0.25° grid scales across monthly and annual resolutions, with trends assessed using the Theil–Sen slope estimator and Mann–Kendall test. By jointly analyzing fire frequency and FRP within a multi-scale framework, this study moves beyond single-indicator descriptions to characterize the co-evolution of fire frequency and FRP, providing an empirical basis for cropland-fire monitoring, early-warning systems, and sustainable land-management strategies.

2. Materials and Methods

2.1. Global Fire Datasets

The active fire data for this study were acquired from the National Aeronautics and Space Administration (NASA) Fire Information for Resource Management System (FIRMS). This dataset provides a continuous, daily record of MODIS Collection 6.1 (C6.1) active fire detections spanning over two decades. The MODIS C6.1 product, delivered in the WGS 1984 geographic coordinate system with a nominal spatial resolution of 1 km at nadir, has been extensively validated and is widely used in global fire monitoring studies [25,32,33]. Data are

distributed in three formats: shapefile (.shp), Google Earth Keyhole Markup Language (.kml), and comma-separated values (.csv) [34,35]. Each fire record includes multiple attributes such as geographic coordinates, fire radiative power (FRP), acquisition date and time, brightness temperature, and detection confidence level. The dataset combines observations from both the Terra (operational since November 2000) and Aqua (operational since July 2002) satellites, providing comprehensive global active fire monitoring coverage [21]. To ensure temporal consistency, this study utilized fire data from both platforms spanning 2003–2022 to analyse spatiotemporal patterns and trend characteristics of global cropland fires. All active fire point products (in .shp format) were bulk-downloaded from the NASA FIRMS data portal (https://firms.modaps.eosdis.nasa.gov/download/, accessed on 9 October 2026). Based on MODIS C6.1 active fire and land-cover data products, the land-cover type at each fire point from 2003 to 2022 was determined using the Extract Values to Points tool in ArcGIS 10.x. Cropland fire data were thereby extracted.

2.2. Global Land Cover Datasets

Land cover information was obtained from the European Space Agency (ESA) Climate Change Initiative (CCI) land cover dataset (https://www.esa-landcover-cci.org/, accessed on 9 October 2026). This product offers global coverage at a spatial resolution of 300 m [36]. The classification scheme follows the Land Cover Classification System of the United Nations Food and Agriculture Organization. For this analysis, the original thematic classes were aggregated into nine consolidated categories: cropland, forest, grassland, shrubland, wetland, water, impervious surfaces, snow/ice, and barren land. The annual time series from 2003 to 2020 was utilized in this study. Since the 2021 and 2022 annual composites were not publicly available at the time of analysis, the 2020 land cover map was applied as a proxy for both subsequent years to maintain temporal continuity in the overlay analysis with fire data.

2.3. Time Series Trend Analysis

Trends in fire activity were analysed using the Theil–Sen (TS) median slope estimator in conjunction with the Mann–Kendall (MK) non-parametric significance test. The Theil–Sen estimator is a robust trend analysis method that was proposed by Theil in 1950 and further refined by Sen in 1968 as a nonparametric method. Because the TS method is primarily calculated using the median of the data, it is less susceptible to the influence of outliers [37]. The TS method is particularly well-suited for analyzing time series with large interannual variations. As this estimator does not directly assess statistical significance, the Mann–Kendall test was applied to evaluate whether observed monotonic trends were statistically significant. The MK test does not require assumptions of normality and performs reliably in the presence of missing values or outliers [38]. This combined TS–MK framework was employed to identify significant long-term trends in cropland fire frequency and FRP over the period of 2003–2022; key results are summarized in Table 1.

Table 1. Time series trend categories.

Slope (TS)	Z (MK)	Trend Feature
Slope > 0	$2.58 < Z$	Highly Significant Increase (HSI)
	$1.96 < Z \leq 2.58$	Significant Increase (SI)
	$1.65 < Z \leq 1.96$	Slightly Significant Increase (SSI)
	$Z \leq 1.65$	No Significant Increase (NSI)

Table 1. *Cont.*

Slope (TS)	Z (MK)	Trend Feature
Slope < 0	$2.58 < Z$	Highly Significant Decrease (HSD)
	$1.96 < Z \leq 2.58$	Significant Decrease (SD)
	$1.65 < Z \leq 1.96$	Slightly Significant Decrease (SSD)
	$Z \leq 1.65$	No Significant Decrease (NSD)

3. Results and Discussion

3.1. Spatiotemporal Patterns and Trend Characteristics of Global Cropland Fires

3.1.1. Distribution Characteristics of Global Cropland Fires

During the 2003–2022 period, global cropland fires reached a cumulative frequency of 2071.59×10^4 with an aggregate fire radiative power (FRP) of 6972.98×10^5 MW, showing pronounced inter-continental spatial heterogeneity. Asia and Africa emerge as the primary hotspots, jointly contributing nearly 70% of global fire points: Asia contributes 35% (731.76×10^4) of the fire frequency and 29% (2050.15×10^5 MW) of the total FRP, while Africa accounts for 34% (714.36×10^4) of the fire frequency and 34% (2391.02×10^5 MW) of the total FRP. South America represents the secondary contributor at 18% (368.27×10^4) of the fire frequency and 25% (1718.14×10^5 MW) of the total FRP, whereas North America, Europe and Oceania each contribute no more than 6% for both metrics. Over the study period, high fire activity persistently concentrates across a set of key nations and regions, including Brazil, Russia, the Democratic Republic of the Congo, Mainland Southeast Asia, India and China. Geographically (Figure 1), fire clusters align closely with the globe's principal agricultural belts: Eastern and Northeastern China, Northwestern India and Mainland Southeast Asia, the Eastern European Plain, equator-intensified Sub-Saharan Africa, Central-Eastern Brazil, and Central-Southern Mexico. By comparison, Oceania features low-magnitude, spatially scattered fire occurrences. Matching the geographic footprint of global cropland extent [39], cropland fires overwhelmingly occupy cultivated land; their spatial decoupling from natural wildfire-prone domains [5,40,41] highlights anthropogenic agricultural management, instead of natural fire regimes, as the principal driver of ignition distributions.

3.1.2. Seasonal Characteristics of Global Cropland Fires

Globally, cropland fires exhibited a distinct bimodal seasonal pattern, with primary peaks occurring during March–April and August–October (Figure 2). The global monthly averages were 8.63×10^4 for fire frequency and 29.05×10^5 MW for FRP. In terms of frequency, April (11.76%) recorded the highest value, followed by September (11.44%) and August (11.35%). For FRP, September (14.53%) ranked first, ahead of August (13.48%) and April (12.27%). These global seasonal rhythms vary substantially across continents. As the primary driver of global cropland fire dynamics, Asia maintains a stable bimodal burning regime during March–April and August–October, which jointly account for over 60% of its continental fires, with monthly averages of 3.05×10^4 fire occurrences and 8.54×10^5 MW FRP. April dominates both fire frequency (18.26%) and FRP (19.63%), with secondary active periods emerging in March–October for fire frequency and March–August for FRP. The strong similarity between Asian and global seasonal fire profiles confirms Asia's leading role in governing worldwide agricultural burning cycles. Asia accommodates over 58% of the global population and sustains approximately 39% of the world's total cropland area, as documented in FAOSTAT statistics. As the continent's core agricultural burning hotspots, India and China predominantly shape the seasonal variability of Asian cropland fires [31]. African cropland fires feature two staggered burning

windows from January–April and July–September, with continental monthly averages of 2.98 × 10^4 for fire frequency and 9.96 × 10^5 MW for FRP. Fire frequency peaks in January (13.50%), while maximum FRP occurs in March (11.98%); this seasonal divergence stems from Africa's cross-hemispheric geographic distribution [13,42]. South American cropland fires are highly concentrated within August–October, a seasonal window contributing over half of the continental fire budget, with synchronized September maxima for both frequency (1.53 × 10^4) and FRP (7.16 × 10^5 MW). This prominent seasonal clustering corresponds to regional dry-season conditions, where southeast trade winds drastically reduce precipitation and promote intensive agricultural burning [29]. North American cropland fires are confined to a spring burning window from March–May, peaking in April (0.55 × 10^4, 1.85 × 10^5 MW), driven largely by pre- and post-harvest residue burning practices across the United States [26]. Europe exhibits a clear bimodal seasonal fire pattern spanning March–April and July–October, with the most intense burning recorded in August (0.40 × 10^4, 1.06 × 10^5 MW), consistent with Eastern European agricultural schedules of spring pre-sowing field cleaning and late summer–autumn stubble removal [43]. Oceania shows a single burning phase concentrated from March to May, where April marks the dominant annual fire peak.

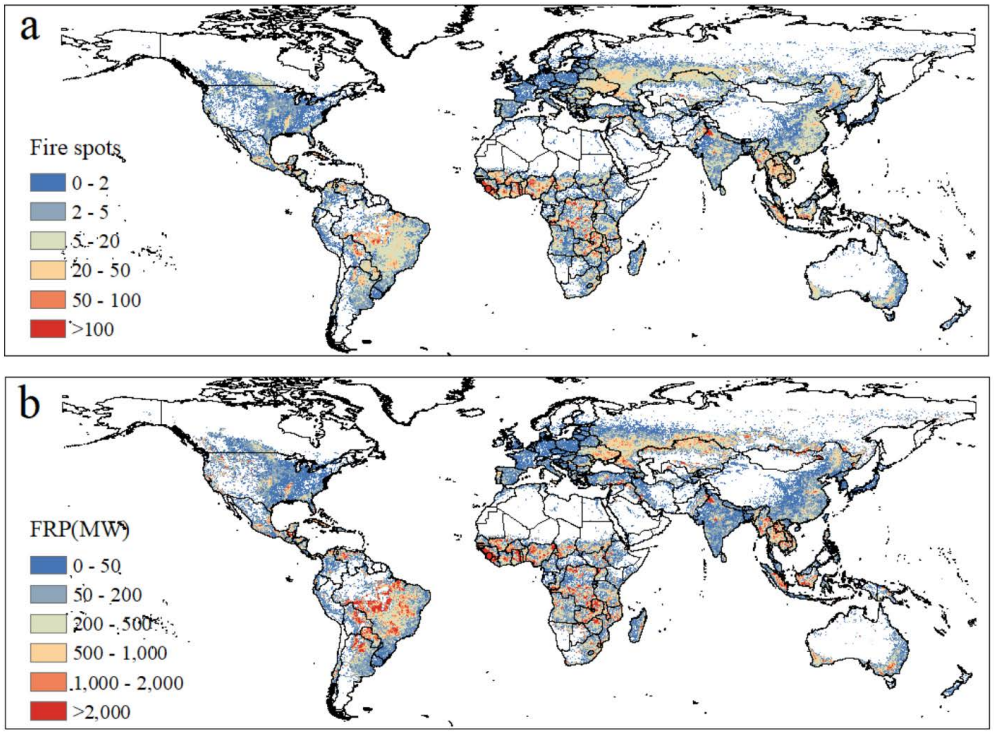


Figure 1. Spatial distribution of the annual number (**a**) and FRP (**b**) of global cropland fires during 2003–2022.

3.1.3. Interannual Characteristics of Global Cropland Fires

Between 2003 and 2022, global cropland fires exhibited a pronounced decreasing trend, with fire frequency declining by 41% and fire radiative power (FRP) declining by 49% (Figure 3). The annual average fire frequency and FRP were 103.58 × 10^4 and 348.65 × 10^5 MW, respectively, with a prominent peak recorded in 2004 (135.31 × 10^4 in fire frequency and 502.77 × 10^5 MW in FRP). Cropland fire trends displayed considerable heterogeneity across continents. In Asia, cropland fires underwent fluctuating decreases, with fire frequency and FRP reduced by 48% and 55%, and the annual averages reached 36.59 × 10^4 and 102.51 × 10^5 MW, respectively. The substantial reductions in Asian cropland fire activities are largely related to

effective governance in China, where straw burning bans and air quality control measures since the mid-2010s have substantially suppressed open agricultural residue burning [31,44,45]. Africa experienced a relatively mild decline, with fire frequency and FRP decreasing by 25% and 31%, and maintained annual averages of 35.72×10^4 and 119.55×10^5 MW. Such a moderate decreasing tendency is potentially associated with cropland expansion and ongoing agricultural intensification across the region [46,47]. South America showed a sharp decline followed by relative stabilization, with fire frequency and FRP dropping by 57% and 66%, and achieved annual averages of 18.41×10^4 and 85.91×10^5 MW. The dramatic reductions in South American cropland fires are likely attributable to the gradual implementation of burning bans in major Brazilian sugarcane planting regions, the transition from manual harvesting to mechanized non-burning harvesting, and the continuous shrinkage of slash-and-burn cultivation in the Amazon [48–50]. North America also presented an overall declining trend, with fire frequency and FRP decreasing by 38% and 44%, and had annual averages of 2.87×10^4 and 4.66×10^5 MW. This downward trend is generally linked to local fire management regulations that restrict open agricultural burning across the United States [26,51]. In comparison, Europe and Oceania maintained persistently low cropland fire levels throughout the study period, with no significant long-term trends.

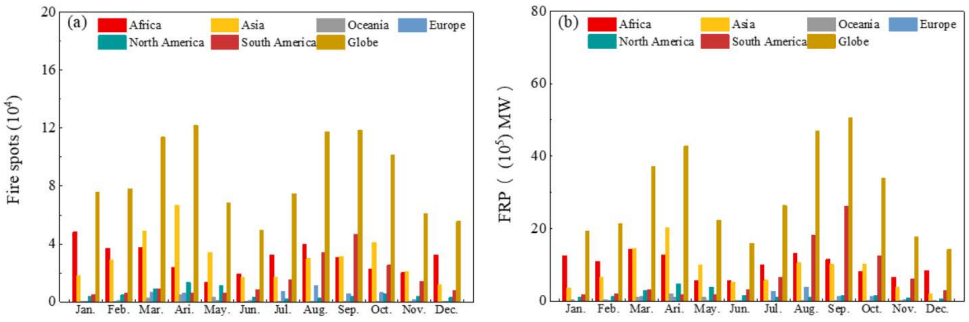


Figure 2. Monthly frequency (**a**) and FRP (**b**) of global cropland fires during 2003–2022.

Time-series analysis revealed a significant global decline in cropland fire activity over the study period: fire frequency decreased at −28,453 yr^{-1} ($p < 0.001$), and FRP declined at −1,268,171 MW yr^{-1} ($p < 0.001$). This global trend, however, masked pronounced continental heterogeneity. South America showed the steepest reductions in both frequency (−10,385 yr^{-1}, $p < 0.001$) and FRP (−613,070 MW yr^{-1}, $p < 0.001$), followed by Asia (−9880 yr^{-1}, $p < 0.001$; −368,992 MW yr^{-1}, $p < 0.001$), Africa (−5738 yr^{-1}, $p < 0.001$; −219,602 MW yr^{-1}, $p < 0.001$), and North America (−1045 yr^{-1}, $p < 0.001$; −38,517 MW yr^{-1}, $p < 0.001$). In contrast, Europe and Oceania, which have predominantly developed economies, showed minimal, statistically non-significant trends, consistent with their historically low cropland fire activity. Spatially, widespread declining fire trends dominated eastern China, Southeast Asia, the Eastern European Plain, equatorial central–southeastern Africa, central-eastern Brazil, and central-southern Mexico (Figure 4). Of particular concern is the concentrated and statistically significant increasing fire trends that were exclusively clustered in key regions including India, Pakistan, the Congo Basin, and northeastern China. These emerging fire hotspots with persistent rising activity deserve targeted attention in future fire monitoring and agricultural management policy design.

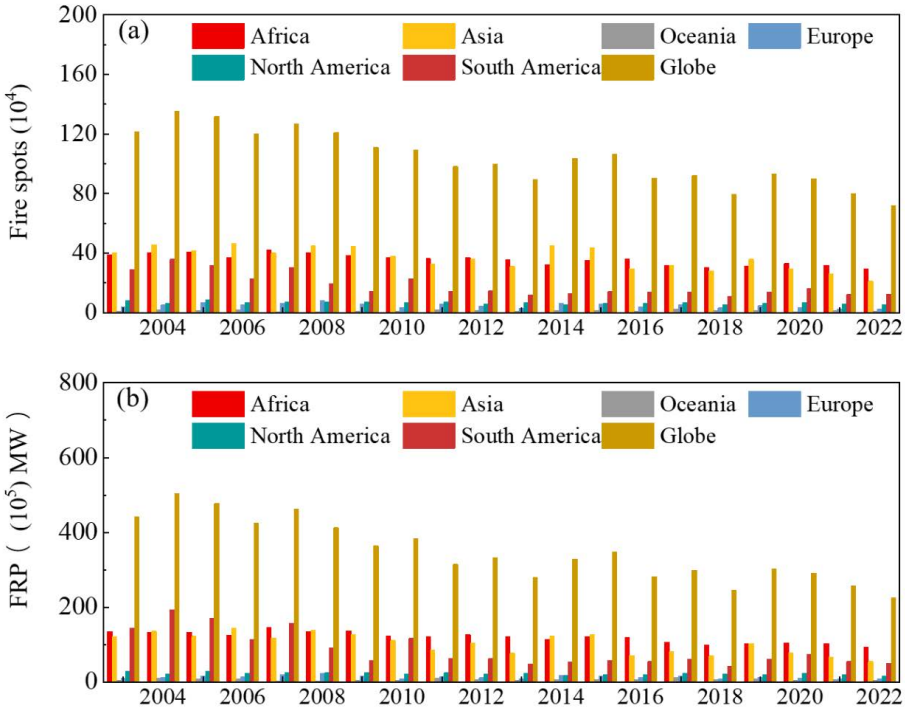


Figure 3. Annual frequency (**a**) and FRP (**b**) of global cropland fires during 2003–2022.

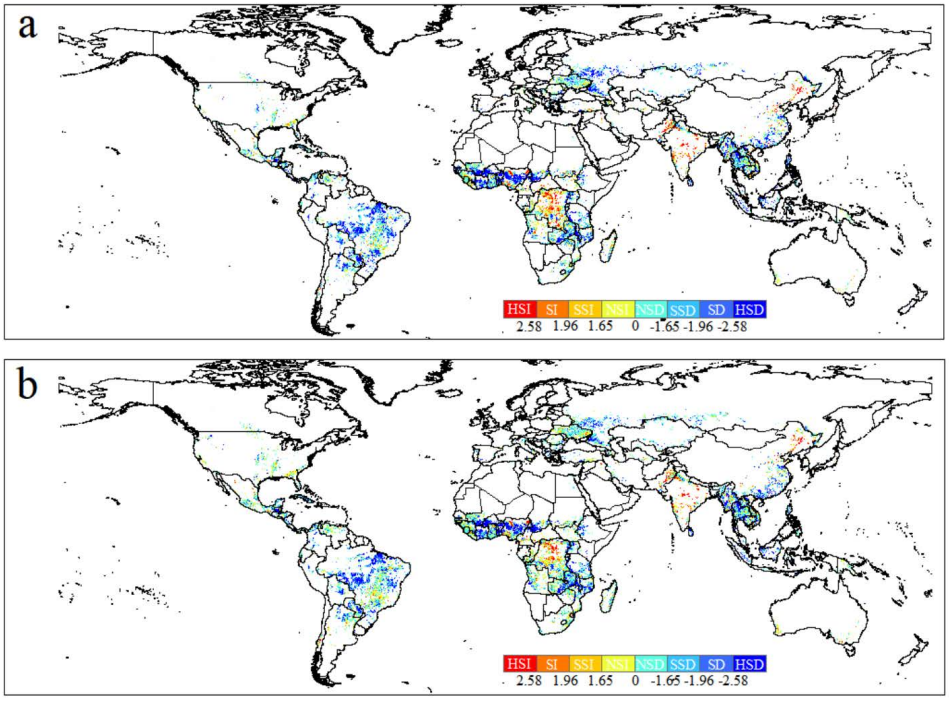


Figure 4. The trend of number (**a**) and FRP (**b**) of global cropland fires during 2003–2022.

3.2. Typical Region Analysis of Cropland Fires

To better characterize the divergent spatiotemporal dynamics of cropland fires at the regional scale, four representative regions—India, Mainland Southeast Asia (MSEA), Brazil, and the Democratic Republic of the Congo (DRC)—were selected for detailed examination. These regions were chosen because they not only constitute globally important cropland fire zones but also epitomize the two opposing evolutionary patterns revealed by our multi-scale analysis: MSEA and Brazil show a downward trend, while fire activities in India and the

Democratic Republic of the Congo are increasing. Placing these contrasting trajectories within a unified analytical framework offers a representative regional perspective that complements the continental- and grid-scale findings and provides a more complete picture of the spatiotemporal heterogeneity of global cropland fires.

3.2.1. Spatiotemporal Evolutionary Patterns of Cropland Fires in MSEA and Brazil

MSEA exhibits two distinct cropland fire regimes: swidden cultivation persists in upland areas, whereas systematic burning of crop residues remains common in lowland agricultural systems [29]. During 2003–2022, cropland fires across the region displayed a pronounced unimodal seasonal pattern, with monthly averages of 0.51×10^4 in fire frequency and 1.49×10^5 MW in FRP. March accounted for the largest share of both fire frequency (34%) and FRP (43%), followed by February (23% and 19%) (Figure 5). These three months together contributed approximately 80% of the annual fire activity, indicating a highly concentrated burning season that largely coincides with the regional dry period, when monthly rainfall typically falls below 20 mm [52]. Spatially, land-clearing fires prevail in highland areas and post-harvest residue burning in lowlands [53], with traditional shifting cultivation remaining widespread across the peninsula [52]. Cropland fires declined significantly from 2003 to 2022, with fire frequency decreasing by 57% and FRP decreasing by 69%. Annual averages were 6.13×10^4 for frequency and 17.90×10^5 MW for FRP, with peak activity occurring in 2004 (9.36×10^4; 28.91×10^5 MW). The declining trends were quantified at rates of -1911 yr^{-1} ($p < 0.001$) for frequency and $-81{,}423$ MW yr^{-1} ($p < 0.001$) for FRP. Over the past two decades, the region has undergone a gradual transition from shifting to permanent agriculture [54].

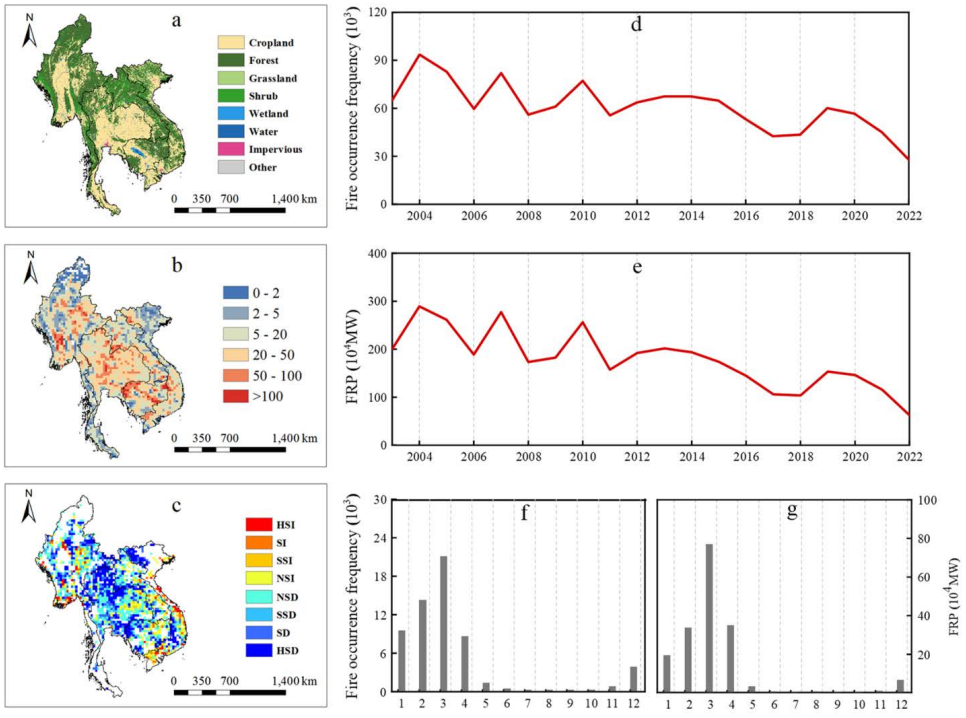


Figure 5. Spatiotemporal dynamics of cropland fires in MSEA, 2003–2022. (**a**) Dominant land cover types. (**b**) Spatial distribution of the annual number of fire spots. (**c**) Interannual trend of cropland fire activity. Annual variations in cropland fire (**d**) frequency and (**e**) FRP. Monthly dynamics of cropland fire (**f**) frequency and (**g**) FRP.

Between 2003 and 2022, cropland fires in Brazil exhibited a distinct unimodal seasonal pattern, with monthly averages of 0.99×10^4 in fire frequency and 4.90×10^5 MW

in FRP. September accounted for the highest shares of both fire frequency (29%) and FRP (34%), followed by August (19% and 22%) and October (16% for both) (Figure 6). Collectively, these three months contributed over 60% of the annual totals, indicating a pronounced seasonal concentration of burning activity. A statistically significant long-term decline in cropland fires was observed over the same period. Fire frequency decreased by 72% and FRP by 81% relative to peak levels. Annual averages reached 11.93×10^4 for frequency and 58.95×10^5 MW for FRP, with peak activity recorded in 2004 (25.82×10^4; 149.13×10^5 MW). Time-series analysis quantified the declines at rates of -8098 yr^{-1} ($p < 0.001$) for frequency and $-494{,}343$ MW yr^{-1} ($p < 0.001$) for FRP. Over recent decades, Brazil has also undergone agricultural modernization and strengthened environmental monitoring and enforcement [2,55].

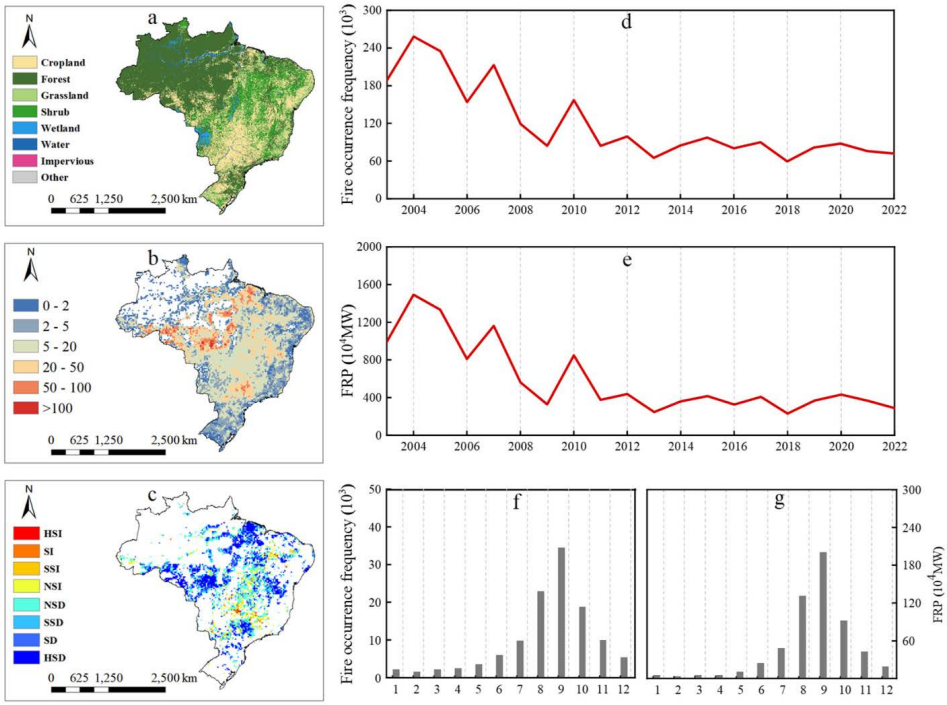


Figure 6. Spatiotemporal dynamics of cropland fires in Brazil, 2003–2022. (**a**) Dominant land cover types. (**b**) Spatial distribution of the annual number of fire spots. (**c**) Interannual trend of cropland fire activity. Annual variations in cropland fire (**d**) frequency and (**e**) FRP. Monthly dynamics of cropland fire (**f**) frequency and (**g**) FRP.

3.2.2. Spatiotemporal Evolutionary Patterns of Cropland Fires in India and DRC

India, a leading global producer of staple crops, generates an estimated 500 million metric tons of crop residue annually, of which approximately 100 million tons are disposed of through open burning [56]. During 2003–2022, cropland fire activity in India exhibited a distinct bimodal seasonal pattern, with peaks in March–May and October–November, alongside a marked spatial concentration in the northwestern states, particularly Punjab and Haryana (Figure 7). National monthly averages were 0.36×10^4 for fire frequency and 0.70×10^5 MW for FRP. November accounted for the highest share of fire occurrences (21%), followed by October (20%) and April (16%); for FRP, April contributed the largest share (23%), ahead of November (17%) and March (16%). The two peaks coincide temporally with the major harvest windows—March–May for wheat and October–November for rice [57]. From 2003 to 2022, both fire frequency and FRP exhibited significant increasing trends, rising by 79% and 74%, respectively. Annual averages reached 4.23×10^4 for frequency and 8.37×10^5 MW for FRP, with peak activity recorded in 2021 (6.22×10^4;

12.74 × 10^5 MW). Time-series analysis confirmed significant annual increases of 1308 yr^{-1} ($p < 0.001$) for frequency and 25,921 MW yr^{-1} ($p < 0.001$) for FRP. Notably, cropland fire activity in India has persisted at high levels despite national policies aimed at restricting crop residue burning [58].

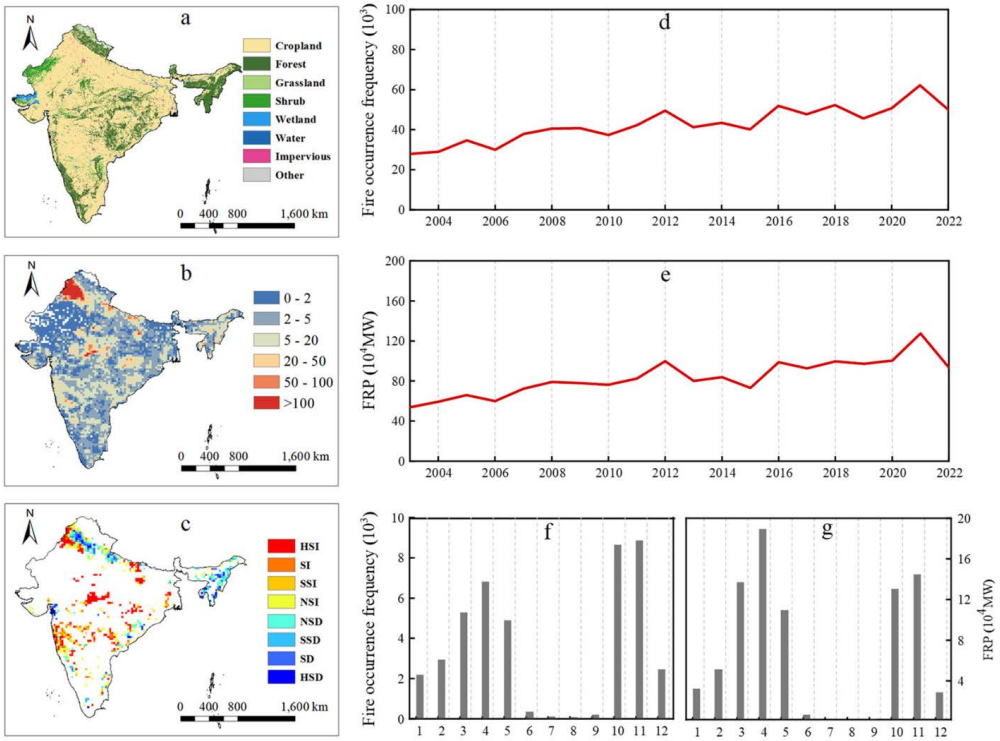


Figure 7. Spatiotemporal dynamics of cropland fires in India, 2003–2022. (**a**) Dominant land cover types. (**b**) Spatial distribution of the annual number of fire spots. (**c**) Interannual trend of cropland fire activity. Annual variations in cropland fire (**d**) frequency and (**e**) FRP. Monthly dynamics of cropland fire (**f**) frequency and (**g**) FRP.

From 2003 to 2022, cropland fires in the DRC exhibited a pronounced unimodal seasonal pattern, in contrast to the bimodal pattern observed in India. Monthly averages were 0.57 × 10^4 for fire frequency and 1.70 × 10^5 MW for FRP. Fire activity peaked in July (21% of annual frequency; 23% of annual FRP), followed by August (20%, 22%) and June (14%, 15%), indicating a burning season concentrated in June–August (Figure 8). Over the study period, cropland fires in the DRC showed an overall increasing trend, with frequency rising by 42% and FRP rising by 19%—a more moderate increase compared to that recorded in India. Annual averages reached 6.83 × 10^4 for frequency and 20.33 × 10^5 MW for FRP, with peak activity recorded in 2016 (8.43 × 10^4; 25.29 × 10^5 MW). Time-series analysis indicated a significant annual increase of 932 yr^{-1} ($p < 0.001$) in frequency, whereas the positive trend in FRP (10,718 MW yr^{-1}) did not reach statistical significance ($p > 0.05$). Slash-and-burn agriculture remains a prevalent traditional practice in the region [59].

3.3. Limitations and Uncertainties

There are some limitations and uncertainties. First, we directly adopted the standardized FIRMS MODIS C6.1 product without additional deduplication of spatially overlapping daily observations. Dual-satellite coverage actually improves the capture of short-lived cropland burning events, and any potential double-counting is regarded as acceptable for our global aggregated analysis. Second, the active-fire data are vector point records, and the land-cover type of each fire point for 2003–2022 was assigned using the Extract Values to

Points tool in ArcGIS (10.x) based on the ESA CCI land-cover product (300 m). Although differences in resolution may introduce potential errors, our study focuses on patterns at the global scale, so the impact on our results is limited. Finally, because the 2021 and 2022 land-cover products were not yet available, the 2020 data was used as a substitute. Given that this two-year window represents only a small fraction of the 20-year record and that annual changes in global cropland extent are generally modest, the resulting influence on the long-term trends is minor and would not change our main conclusions. These factors constitute multiple sources of uncertainty in research on cropland fires. Despite these challenges, this study provides valuable insights into the spatiotemporal distribution patterns and dynamic characteristics of cropland fires at the national, regional, and global scales.

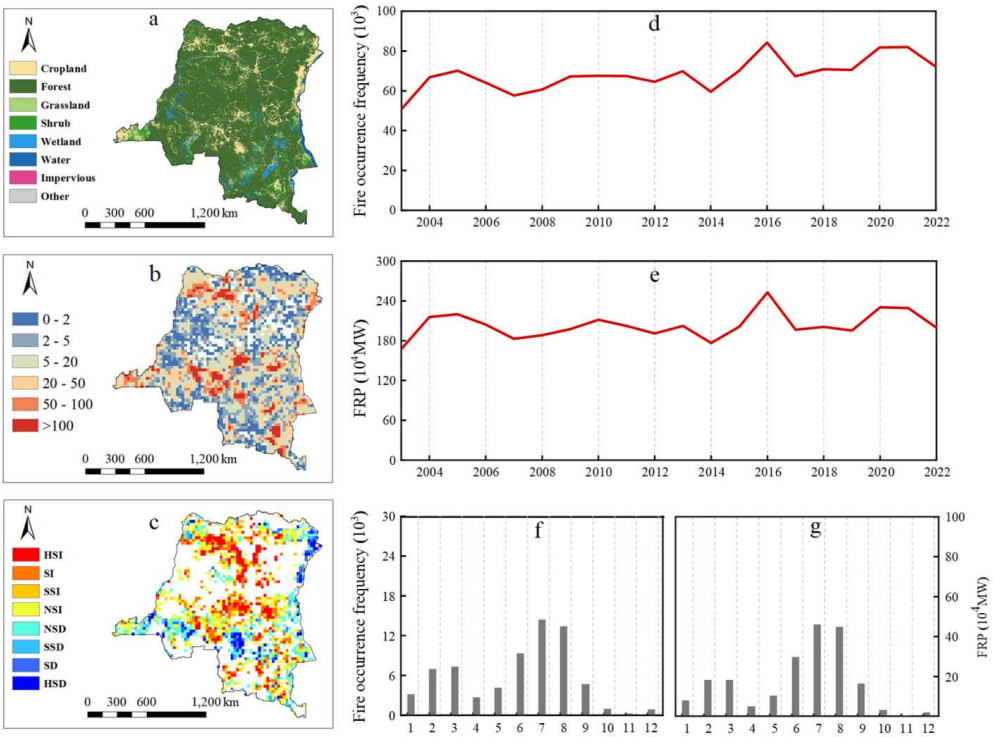


Figure 8. Spatiotemporal dynamics of cropland fires in DRC, 2003–2022. (**a**) Dominant land cover types. (**b**) Spatial distribution of the annual number of fire spots. (**c**) Interannual trend of cropland fire activity. Annual variations in cropland fire (**d**) frequency and (**e**) FRP. Monthly dynamics of cropland fire (**f**) frequency and (**g**) FRP.

4. Conclusions

Drawing on MODIS Collection 6.1 active fire products and land-cover datasets, this study systematically characterized the spatiotemporal patterns and evolutionary dynamics of global cropland fires during 2003–2022, using fire frequency and fire radiative power (FRP) as dual indicators across global, continental, national, and 0.25° grid scales. Our results confirm the hypothesis that global cropland fire activity exhibits pronounced spatial heterogeneity. Spatially, cropland fires were predominantly concentrated in Asia and Africa, together accounting for approximately 70% of global fire activity, with additional hotspots in South America. Temporally, a bimodal seasonal pattern emerged at the global aggregate level, with peaks in March–April and August–October, coinciding with regional harvest calendars and dry-season burning in the two hemispheres. Over the study period, global fire frequency and FRP declined significantly, by 41% and 49%, respectively ($p < 0.001$). South America, Asia, and Africa experienced prominent reductions, whereas Europe and Oceania maintained persistently low fire activity without significant trends. In

particular, India, Pakistan, DRC and northeastern China are still on the rise, which deserves further attention. This study provides a refined, multi-scale portrait of global cropland fire spatiotemporal heterogeneity, offering a fundamental observational baseline for future regional fire monitoring and targeted agricultural fire management worldwide.

Author Contributions: Conceptualization, C.L.; methodology, C.L. and Z.L.; software, C.L.; validation, C.L.; formal analysis, C.L.; investigation, C.L.; resources, C.L.; data curation, C.L. and Z.L; writing—original draft preparation, C.L.; writing—review and editing, C.L., Z.F. and G.L.; visualization, C.L.; supervision, Z.F. and G.L.; project administration, Z.F. and G.L.; funding acquisition, Z.F. and G.L. All authors have read and agreed to the published version of the manuscript.

Funding: This paper was supported by the National Natural Science Foundation of China (42262010 and 42130508) and the Natural Science Foundation of Inner Mongolia Autonomous Region (2026MS0443).

Data Availability Statement: Some or all data and models that support the findings of this study are available from the corresponding author upon reasonable request.

Conflicts of Interest: The authors declare no conflicts of interest.

References

1. Lian, C.; Xiao, C.; Feng, Z.; Ma, Q. Accelerating decline of wildfires in China in the 21st century. *Front. For. Glob. Change* **2024**, *6*, 1252587. [CrossRef]
2. Aragao, L.; Anderson, L.O.; Fonseca, M.G.; Rosan, T.M.; Vedovato, L.B.; Wagner, F.H.; Silva, C.V.J.; Silva Junior, C.H.L.; Arai, E.; Aguiar, A.P.; et al. 21st Century drought-related fires counteract the decline of Amazon deforestation carbon emissions. *Nat. Commun.* **2018**, *9*, 536. [CrossRef] [PubMed]
3. Elia, M.; D'Este, M.; Ascoli, D.; Giannico, V.; Spano, G.; Ganga, A.; Colangelo, G.; Lafortezza, R.; Sanesi, G. Estimating the probability of wildfire occurrence in Mediterranean landscapes using Artificial Neural Networks. *Environ. Impact Assess. Rev.* **2020**, *85*, 106474. [CrossRef]
4. Xia, L.; Yang, Z.; Yang, Y.; Han, L.; Jia, C.; Li, J.; Fan, W.; Liu, R. Assessing the spatiotemporal dynamics of wildfire drivers in Southeast Asia: An explainable spatial machine learning framework. *Environ. Impact Assess. Rev.* **2026**, *118*, 108337. [CrossRef]
5. Bowman, D.; Kolden, C.A.; Abatzoglou, J.T.; Johnston, F.H.; van der Werf, G.R.; Flannigan, M. Vegetation fires in the Anthropocene. *Nat. Rev. Earth Environ.* **2020**, *1*, 500–515. [CrossRef]
6. Wang, J.; Wang, X. A triumph of reducing carbon emission by banning open straw burning. *Sci. Bull.* **2023**, *68*, 18–20. [CrossRef] [PubMed]
7. Jones, M.W.; Abatzoglou, J.T.; Veraverbeke, S.; Andela, N.; Lasslop, G.; Forkel, M.; Smith, A.J.P.; Burton, C.; Betts, R.A.; van der Werf, G.R.; et al. Global and Regional Trends and Drivers of Fire Under Climate Change. *Rev. Geophys.* **2022**, *60*, e2020RG000726. [CrossRef]
8. Earl, N.; Simmonds, I. Spatial and Temporal Variability and Trends in 2001-2016 Global Fire Activity. *J. Geophys. Res.-Atmos.* **2018**, *123*, 2524–2536. [CrossRef]
9. Rajasekhar Balasubramanian, S.W.S. Impact of Forest Fires on Regional Air Quality in Southeast Asia. *Chin. J. Geochem.* **2006**, *25*, 221–222. [CrossRef]
10. Arbex, M.A.; Martins, L.C.; de Oliveira, R.C.; Pereira, L.A.; Arbex, F.F.; Cancado, J.E.; Saldiva, P.H.; Braga, A.L. Air pollution from biomass burning and asthma hospital admissions in a sugar cane plantation area in Brazil. *J. Epidemiol. Community Health* **2007**, *61*, 395–400. [CrossRef] [PubMed]
11. Lin, H.; Wang, X.; Qian, Z.M.; Guo, S.; Yao, Z.; Vaughn, M.G.; Dong, G.; Liu, T.; Xiao, J.; Li, X.; et al. Daily exceedance concentration hours: A novel indicator to measure acute cardiovascular effects of PM(2.5) in six Chinese subtropical cities. *Environ. Int.* **2018**, *111*, 117–123. [CrossRef] [PubMed]
12. Pun, V.C.; Kazemiparkouhi, F.; Manjourides, J.; Suh, H.H. Long-Term PM2.5 Exposure and Respiratory, Cancer, and Cardiovascular Mortality in Older US Adults. *Am. J. Epidemiol.* **2017**, *186*, 961–969. [CrossRef] [PubMed]
13. Hall, J.V.; Argueta, F.; Zubkova, M.; Chen, Y.; Randerson, J.T.; Giglio, L. GloCAB: Global cropland burned area from mid-2002 to 2020. *Earth Syst. Sci. Data* **2024**, *16*, 867–885. [CrossRef]
14. Yin, S. Biomass burning spatiotemporal variations over South and Southeast Asia. *Environ. Int.* **2020**, *145*, 106153. [CrossRef] [PubMed]
15. Lelieveld, J.; Evans, J.S.; Fnais, M.; Giannadaki, D.; Pozzer, A. The contribution of outdoor air pollution sources to premature mortality on a global scale. *Nature* **2015**, *525*, 367–384. [CrossRef] [PubMed]

16. Arunrat, N.; Kongsurakan, P.; Solomon, L.W.; Sereenonchai, S. Fire Impacts on Soil Properties and Implications for Sustainability in Rotational Shifting Cultivation: A Review. *Agriculture* **2024**, *14*, 1660. [CrossRef]
17. Fachin, P.A.; Thomaz, E.L.; Fernandes, N.F.; Coelho Netto, A.L. Seven decades of Atlantic rainforest conversion to slash-and-burn agriculture: Effects on soil's physical properties. *J. Environ. Manag.* **2024**, *350*, 119682. [CrossRef] [PubMed]
18. Schroeder, W.; Oliva, P.; Giglio, L.; Csiszar, I.A. The New VIIRS 375 m active fire detection data product: Algorithm description and initial assessment. *Remote Sens. Environ.* **2014**, *143*, 85–96. [CrossRef]
19. Giglio, L.; Boschetti, L.; Roy, D.P.; Humber, M.L.; Justice, C.O. The Collection 6 MODIS burned area mapping algorithm and product. *Remote Sens. Environ.* **2018**, *217*, 72–85. [CrossRef] [PubMed]
20. Giglio, L.; Randerson, J.T.; van der Werf, G.R. Analysis of daily, monthly, and annual burned area using the fourth-generation global fire emissions database (GFED4). *J. Geophys. Res. Biogeosci.* **2013**, *118*, 317–328. [CrossRef]
21. Giglio, L.; Schroeder, W.; Justice, C.O. The collection 6 MODIS active fire detection algorithm and fire products. *Remote Sens. Environ.* **2016**, *178*, 31–41. [CrossRef] [PubMed]
22. Morgan, P.; Hardy, C.C.; Swetnam, T.W.; Rollins, M.G.; Long, D.G. Mapping fire regimes across time and space: Understanding coarse and fine-scale fire patterns. *Int. J. Wildland Fire* **2001**, *10*, 329–342. [CrossRef]
23. Yin, S.; Guo, M.; Wang, X.; Yamamoto, H.; Ou, W. Spatiotemporal variation and distribution characteristics of crop residue burning in China from 2001 to 2018. *Environ. Pollut.* **2021**, *268*, 115849. [CrossRef] [PubMed]
24. Zhuang, Y.; Li, R.Y.; Yang, H.; Chen, D.L.; Chen, Z.Y.; Gao, B.B.; He, B. Understanding Temporal and Spatial Distribution of Crop Residue Burning in China from 2003 to 2017 Using MODIS Data. *Remote Sens.* **2018**, *10*, 390. [CrossRef]
25. Lian, C.; Xiao, C.; Feng, Z. Spatiotemporal Characteristics and Regional Variations of Active Fires in China since 2001. *Remote Sens.* **2023**, *15*, 54. [CrossRef]
26. McCarty, J.L.; Korontzi, S.; Justice, C.O.; Loboda, T. The spatial and temporal distribution of crop residue burning in the contiguous United States. *Sci. Total Environ.* **2009**, *407*, 5701–5712. [CrossRef] [PubMed]
27. Wei, X.; Wang, G.; Chen, T.; Hagan, D.F.T.; Ullah, W. A Spatio-Temporal Analysis of Active Fires over China during 2003–2016. *Remote Sens.* **2020**, *12*, 1787. [CrossRef]
28. Yang, X.; Zhao, C.; Zhao, W.; Fan, H.; Yang, Y. Characterization of global fire activity and its spatiotemporal patterns for different land cover types from 2001 to 2020. *Environ. Res.* **2023**, *227*, 115746. [CrossRef] [PubMed]
29. Li, P.; Xiao, C.; Feng, Z.; Li, W.; Zhang, X. Occurrence frequencies and regional variations in Visible Infrared Imaging Radiometer Suite (VIIRS) global active fires. *Glob. Change Biol.* **2020**, *26*, 2970–2987. [CrossRef] [PubMed]
30. Giglio, L.; Csiszar, I.; Justice, C.O. Global distribution and seasonality of active fires as observed with the Terra and Aqua Moderate Resolution Imaging Spectroradiometer (MODIS) sensors. *J. Geophys. Res.-Biogeosciences* **2006**, *111*, G02016. [CrossRef]
31. Lian, C.; Li, P.; Feng, Z. Accelerated reduction in China's cropland fires against the background of policy enhancement. *Environ. Impact Assess. Rev.* **2024**, *106*, 107512. [CrossRef]
32. Li, W.; Li, P.; Feng, Z. Delineating Fire-Hazardous Areas and Fire-Induced Patterns Based on Visible Infrared Imaging Radiometer Suite (VIIRS) Active Fires in Northeast China. *Remote Sens.* **2022**, *14*, 5115. [CrossRef]
33. Xiang, M.; Xiao, C.; Feng, Z.; Ma, Q. Global distribution, trends and types of active fire occurrences. *Sci. Total Environ.* **2023**, *902*, 166456. [CrossRef] [PubMed]
34. Davies, D.K.; Ilavajhala, S.; Wong, M.M.; Justice, C.O. Fire Information for Resource Management System: Archiving and Distributing MODIS Active Fire Data. *IEEE Trans. Geosci. Remote Sens.* **2009**, *47*, 72–79. [CrossRef]
35. Xiao, C.; Feng, Z.; Li, P. Active fires show an increasing elevation trend in the tropical highlands. *Glob. Change Biol.* **2022**, *28*, 2790–2803. [CrossRef] [PubMed]
36. European Space Agency Climate Change Initiative Land Cover Project (Land Cover CCI). *Land Cover CCI Product User Guide Version 2.0*; UCL-Geomatics: Louvain-la-Neuve, Belgium, 2017.
37. Sen, P.K. Estimates of the Regression Coefficient Based on Kendall's Tau. *J. Am. Stat. Assoc.* **1968**, *63*, 1379–1389. [CrossRef]
38. Forthofer, R.N.; Lehnen, R.G. Rank Correlation Methods. In *Public Program Analysis: A New Categorical Data Approach*; Forthofer, R.N., Lehnen, R.G., Eds.; Springer: Boston, MA, USA, 1981; pp. 146–163.
39. Potapov, P.; Turubanova, S.; Hansen, M.C.; Tyukavina, A.; Zalles, V.; Khan, A.; Song, X.-P.; Pickens, A.; Shen, Q.; Cortez, J. Global maps of cropland extent and change show accelerated cropland expansion in the twenty-first century. *Nat. Food* **2022**, *3*, 19–28. [CrossRef] [PubMed]
40. Burke, M.; Childs, M.L.; de la Cuesta, B.; Qiu, M.; Li, J.; Gould, C.F.; Heft-Neal, S.; Wara, M. The contribution of wildfire to PM2.5 trends in the USA. *Nature* **2023**, *622*, 761–766. [CrossRef] [PubMed]
41. Jolly, W.M.; Cochrane, M.A.; Freeborn, P.H.; Holden, Z.A.; Brown, T.J.; Williamson, G.J.; Bowman, D.M.J.S. Climate-induced variations in global wildfire danger from 1979 to 2013. *Nat. Commun.* **2015**, *6*, 7537. [CrossRef] [PubMed]
42. Xu, C.; You, C. Agricultural expansion dominates rapid increases in cropland fires in Asia. *Environ. Int.* **2023**, *179*, 108189. [CrossRef] [PubMed]

43. Hall, J.V.; Zibtsev, S.V.; Giglio, L.; Skakun, S.; Myroniuk, V.; Zhuravel, O.; Goldammer, J.G.; Kussul, N. Environmental and political implications of underestimated cropland burning in Ukraine. *Environ. Res. Lett.* **2021**, *16*, 064019. [CrossRef] [PubMed]
44. Lian, C.; Feng, Z. Dynamics of PM2.5 Emissions from Cropland Fires in Typical Regions of China and Its Impact on Air Quality. *Fire* **2026**, *9*, 46. [CrossRef]
45. Huang, L.; Zhu, Y.; Wang, Q.; Zhu, A.; Liu, Z.; Wang, Y.; Allen, D.T.; Li, L. Assessment of the effects of straw burning bans in China: Emissions, air quality, and health impacts. *Sci. Total Environ.* **2021**, *789*, 147935. [CrossRef] [PubMed]
46. Andela, N.; van der Werf, G.R. Recent trends in African fires driven by cropland expansion and El Niño to La Niña transition. *Nat. Clim. Change* **2014**, *4*, 791–795. [CrossRef]
47. Yu, Y.; Mao, J.; Thornton, P.E.; Notaro, M.; Wullschleger, S.D.; Shi, X.; Hoffman, F.M.; Wang, Y. Quantifying the drivers and predictability of seasonal changes in African fire. *Nat. Commun.* **2020**, *11*, 2893. [CrossRef] [PubMed]
48. Jakovac, C.C.; Dutrieux, L.P.; Siti, L.; Peña-Claros, M.; Bongers, F. Spatial and temporal dynamics of shifting cultivation in the middle-Amazonas river: Expansion and intensification. *PLoS ONE* **2017**, *12*, e0181092. [CrossRef] [PubMed]
49. Galdos, M.; Cavalett, O.; Seabra, J.E.A.; Nogueira, L.A.H.; Bonomi, A. Trends in global warming and human health impacts related to Brazilian sugarcane ethanol production considering black carbon emissions. *Appl. Energy* **2013**, *104*, 576–582. [CrossRef]
50. Aguiar, D.A.; Rudorff, B.F.T.; Silva, W.F.; Adami, M.; Mello, M.P. Remote Sensing Images in Support of Environmental Protocol: Monitoring the Sugarcane Harvest in São Paulo State, Brazil. *Remote Sens.* **2011**, *3*, 2682–2703. [CrossRef]
51. Lin, H.W.; McCarty, J.L.; Wang, D.; Rogers, B.M.; Morton, D.C.; Collatz, G.J.; Jin, Y.; Randerson, J.T. Management and climate contributions to satellite-derived active fire trends in the contiguous United States. *J. Geophys. Res. Biogeosci.* **2014**, *119*, 645–660. [CrossRef] [PubMed]
52. Li, P.; Feng, Z.; Xiao, C.; Khampheng, B.; Liu, Y. Detecting and mapping annual newly-burned plots (NBP) of swiddening using historical Landsat data in Montane Mainland Southeast Asia (MMSEA) during 1988-2016. *J. Geogr. Sci.* **2018**, *28*, 1307–1328. [CrossRef]
53. Li, P.; Feng, Z. Extent and Area of Swidden in Montane Mainland Southeast Asia: Estimation by Multi-Step Thresholds with Landsat-8 OLI Data. *Remote Sens.* **2016**, *8*, 44. [CrossRef]
54. Yin, S.; Wang, X.; Zhang, X.; Guo, M.; Miura, M.; Xiao, Y. Influence of biomass burning on local air pollution in mainland Southeast Asia from 2001 to 2016. *Environ. Pollut.* **2019**, *254*, 112949. [CrossRef] [PubMed]
55. Laurance, W.F.; Sayer, J.; Cassman, K.G. Agricultural expansion and its impacts on tropical nature. *Trends Ecol. Evol.* **2014**, *29*, 107–116. [CrossRef] [PubMed]
56. Lan, R.; Eastham, S.D.; Liu, T.; Norford, L.K.; Barrett, S.R.H. Air quality impacts of crop residue burning in India and mitigation alternatives. *Nat. Commun.* **2022**, *13*, 6537. [CrossRef] [PubMed]
57. Gustafsson, Ö.; Kruså, M.; Zencak, Z.; Sheesley, R.J.; Granat, L.; Engström, E.; Praveen, P.S.; Rao, P.S.P.; Leck, C.; Rodhe, H. Brown Clouds over South Asia: Biomass or Fossil Fuel Combustion? *Science* **2009**, *323*, 495–498. [CrossRef] [PubMed]
58. Shyamsundar, P.; Springer, N.P.; Tallis, H.; Polasky, S.; Jat, M.L.; Sidhu, H.S.; Krishnapriya, P.P.; Skiba, N.; Ginn, W.; Ahuja, V.; et al. Fields on fire: Alternatives to crop residue burning in India. *Science* **2019**, *365*, 536–538. [CrossRef] [PubMed]
59. Potapov, P.V.; Turubanova, S.A.; Hansen, M.C.; Adusei, B.; Broich, M.; Altstatt, A.; Mane, L.; Justice, C.O. Quantifying forest cover loss in Democratic Republic of the Congo, 2000–2010, with Landsat ETM+ data. *Remote Sens. Environ.* **2012**, *122*, 106–116. [CrossRef]

Disclaimer/Publisher's Note: The statements, opinions and data contained in all publications are solely those of the individual author(s) and contributor(s) and not of MDPI and/or the editor(s). MDPI and/or the editor(s) disclaim responsibility for any injury to people or property resulting from any ideas, methods, instructions or products referred to in the content.